ACS APPLIED OPTICAL MATERIALS

pubs.acs.org/acsaom Article

Luminescent Analysis of Eu^{3+} and Tb^{3+} Flufenamate Complexes Doped in PMMA Polymer: Unexpected Terbium Green Emission under Sunlight Exposure

Israel P. Assunção,* Israel F. Costa, Paulo R. S. Santos, Ercules E. S. Teotonio, Maria Claudia F. C. Felinto, Ulrich Kynast, Wagner M. Faustino, Oscar Malta, and Hermi F. Brito*

Cite This: ACS Appl. Opt. Mater. 2023, 1, 354−366 Read Online

ACCESS | Metrics & More | Article Recommendations | Supporting Information

ABSTRACT: The design of efficient luminescent lanthanide materials with a wide range of different excitation wavelengths in the UVA, UVB, and UVC regions, as well as under sunlight exposure, is highly desirable for application as molecular light-converting devices. In this work, $[Ln(fluf)_3(L)]$ complexes (Ln^{3+}: Eu, Gd, and Tb) and doped PMMA:(1%)$Tb(fluf)_3(L)$ films, where fluf stands for the flufenamate ligand and L is H_2O, phen, tppo, topo, and dpso, were successfully prepared by a facile one-pot method, and their photophysical properties were also investigated. The Ln^{3+} compounds were characterized by elemental analysis, Fourier transform infrared absorption spectroscopy, thermogravimetric analysis, X-ray powder diffraction, and diffuse reflectance spectroscopy techniques. The Eu^{3+} complexes present very weak emission intensities at 300 K temperature, showing very low intrinsic quantum yield (Q_{Eu}^{Eu}) values due to a highly operative luminescence quenching by a low-lying ligand to metal charge transfer state. However, these values are significantly increased when obtained at low temperature (77 K). For Tb^{3+} complexes and the doped PMMA, polymeric films revealed an unprecedented bright emission under excitation at UVA, UVB, and UVC radiation. In addition, the doped polymers under sunlight exposure show the characteristic $^5D_4 \rightarrow {}^7F_{6-0}$ transitions of the Tb^{3+} ion, exhibiting green emission color. These luminescent doped polymeric materials act as efficient energy harvesters and converters. Hence, the optical results show that the PMMA:(1%)$Tb(fluf)_3(L)$ photonic materials are highly versatile and desirable, presenting suitable application as efficient light-converting molecular devices and as luminescent solar concentrators.

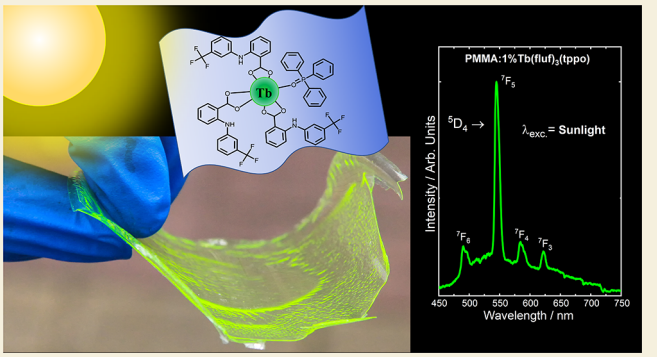

KEYWORDS: *photoluminescence, lanthanide complexes, flufenamates, energy transfer, LMCT, sunlight-emitting materials*

1. INTRODUCTION

Luminescent solar concentrators (LSCs) are a class of material that consists of a planar waveguide (glass or polymer-based), allowing the conversion of sunlight into electricity when attached to a voltaic cell.[1] Indeed, LSC research goes back more than 40 years ago[2,3] but has significantly increased in the past decade with the rising fossil-fuel prices and the awareness of their environmental hazards.

In this way, trivalent lanthanide (Ln^{3+}) coordination compounds have attracted much attention mainly due to their narrow emission bands and long lifetimes assigned to the 4f−4f transitions and considerable distance between the excitation and emission maxima from the organic ligand and the metal ion transitions, avoiding reabsorption loss processes. In the last decades, Ln^{3+}-based luminescent materials have also been applied in different areas, mainly as optical markers,[4,5] luminescent probes for medical diagnosis,[6,7] temperature sensors,[8,9] hybrid materials,[10,11] as well as the aforementioned LSCs.[1,12]

Notably, the unique photoluminescent properties of the Ln^{3+} ions depend significantly on their intrinsic energy level structures. Moreover, the intraconfigurational 4f transitions are forbidden by the Laporte rule, leading thus to very low molar absorptivity coefficients. In this way, concerning the Ln^{3+} coordination compounds, organic ligands can play an important role as efficient luminescent sensitizers, absorbing and efficiently transferring the energy to the metal ions.[13]

Received: August 25, 2022
Accepted: October 28, 2022
Published: November 16, 2022

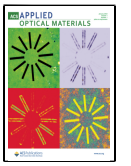

One of the most common intramolecular energy transfer processes from the ligand to the lanthanide ion (L → Ln^{3+}) usually takes place from the strong light absorption by the ligands from the ground to excited singlet states ($S_0 \rightarrow S_n$). Subsequently, the first excited S_1 state decays in a nonradiative pathway through intersystem crossing to a lower triplet state ($S_1 \rightarrow T_1$). Thus, the excited T_1 state transfers the energy via a nonradiative process to the Ln^{3+} excited levels, emitting light with a characteristic emission wavelength.[13−15] Nevertheless, competitive deactivation processes can depopulate the main emitting levels of the Ln^{3+} ions, affecting the emission quantum yield. Such luminescence quenching can occur via vibronic coupling with high-energy oscillators like C−H, N−H, and mainly O−H stretching modes from the ligands.[16−18]

Furthermore, the ligand to metal charge transfer (LMCT) states at low energy can play an essential role as an efficient deactivation pathway, as pointed out by the seminal studies of Jørgensen in 1962.[19,20] The LMCT relative position depends mainly on the oxidation potential of the ligands and the electron affinity of the lanthanide ion,[16] among which the Eu^{3+} species constitute a particular case due to its possibility of achieving a half-filled shell configuration. Generally, this spectroscopic behavior has been observed for several Eu^{3+} complexes containing β-diketonates, carboxylates, dithiocarbamates, etc.[21−24] On the other hand, to the best of our knowledge, there are no Tb^{3+} complexes that exhibit LMCT at low energies, indicating that this state generally does not interfere in its photoluminescence process. The main $^5D_0$ (Eu^{3+}) and $^5D_4$ (Tb^{3+}) emitting energy levels are located at around 17290 and 20400 cm^{-1}, respectively.[25] Therefore, their analogous compounds present quite different emission quantum yields, mainly when Eu^{3+} compounds contain low-energy LMCT states.

Among carboxylate organic ligands, those based on the so-called nonsteroidal anti-inflammatory drugs (NSAIDs) have recently received particular attention as luminescent sensitizers for Ln^{3+} ions.[26,27] The studies indicated that the Tb^{3+} complexes with the monoanion of the so-called flufenamic acid (hereafter fluf) exhibit the highest luminescence. This ligand can sensitize Ln^{3+} ions under excitation as high as 400 nm, which is a desirable feature for technological application. Nevertheless, while several Eu^{3+}-based complexes are suitable for this purpose,[28,29] Tb^{3+}-based systems are relatively scarce in this sense.

Polymers usually present intrinsic features like mechanical strength, ease and relatively low cost of production, flexibility, application versatility, etc.[11,30] For example, the poly(methyl methacrylate) (PMMA) polymer is one of the most widely employed mainly due to its excellent mechanical and optical properties[11] and high light transmittance, chemical resistance, and low optical absorption.[10] In this way, doping luminescent species such as Ln^{3+} complexes into the PMMA matrix may lead to hybrid materials with new properties arising from the synergy of both components.[11,30,31]

Therefore, this work investigated the synthesis and spectroscopic properties of Ln^{3+} flufenamates (Ln^{3+}: Eu, Gd, and Tb) containing different neutral organic molecules, such as 1,10-phenanthroline (phen), triphenylphosphinoxide (tppo), trioctylphosphinoxide (topo), and diphenylsulfoxide (dpso), acting as ancillary ligands (Figure 1). In addition, the photoluminescent behavior of PMMA:(1%)Ln^{3+} flufenamate complexes (Eu^{3+} and Tb^{3+}) was studied and revealed absolutely opposite results. The PMMA:Eu^{3+} complexes do not exhibit luminescence (except for topo ligand) at room temperature due to the presence of the LMCT band, which efficiently quenches their luminescence. Conversely, the PMMA:(1%)Tb^{3+} complexes show a bright green emission under irradiation at UVA, UVB, and UVC regions as well as when exposed to sunlight radiation, suggesting that these luminescent materials could be applied as efficient emitters.

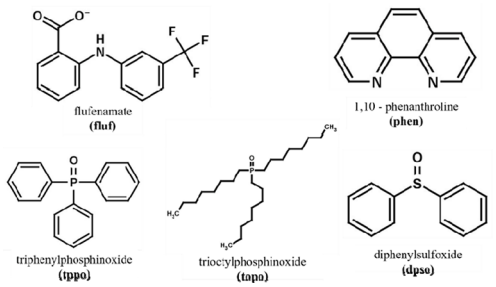

Figure 1. Flufenamate (fluf) main ligand and 1,10-phenanthroline (phen), triphenylphosphinoxide (tppo), trioctylphosphinoxide (topo), and diphenylsulfoxide (dpso) coligand structures.

2. EXPERIMENTAL PROCEDURE

2.1. Synthesis of the [Ln(fluf)$_3$(L)] Complexes

The Ln^{3+} chlorides (Ln^{3+}: Eu, Gd, and Tb) were synthesized according to the literature[32] by the reaction of the corresponding oxide (Ln_2O_3, CSTARM, and Tb_4O_7 Rhodia) with HCl (37% w/w, Vetec). After this step, the $LnCl_3{\cdot}6H_2O$ aqueous solution was filtered and the solvent evaporated, leading to a crystalline solid that was dried and stored in a desiccator under reduced pressure. It is noteworthy that $TbCl_3{\cdot}6H_2O$ was prepared by using a brownish precursor Tb_4O_7 oxide with HCl and hydrogen peroxide (H_2O_2) to reduce the Tb^{IV} to Tb^{3+} species until obtaining a transparent solution.

The [Ln(fluf)$_3$(L)] coordination compounds were synthesized via a one-pot synthesis containing lanthanide chlorides, the fluf ligand, and the correspondingt neutral ancillary ligands (phen, tppo, topo, and dpso) in an ethanolic solution. The deprotonation reaction of the flufenamic acid was performed by using a concentrated ammonia solution until pH ∼7. The $LnCl_3{\cdot}6H_2O$ solid was previously dissolved in EtOH and added dropwise to the fluf/L homogeneous mixture in a Ln^{3+}:fluf:L ratio of 1:3:1 for all [Ln(fluf)$_3$(L)] complexes. The reaction mixture was heated at 80 °C under stirring for 2 h. Subsequently, 10 mL of H_2O was added to yield solid samples. After that, the heterogeneous mixture was filtered, dried in an oven at 50 °C, and stored in a desiccator. The final products are solids, except for the topo complexes obtained as viscous oil. All Ln^{3+} complexes are soluble in methanol, ethanol, isopropyl alcohol, acetone, and DMSO, presenting the general formula [Ln(fluf)$_3$(L)], where Ln^{3+}: Eu, Gd, and Tb and L: phen, tppo, topo, and dpso. In general, the percent yield for the reactions was about 60%.

The incorporation of the Ln^{3+}-flufenamates (Eu and Tb) into the PMMA matrix was achieved by the complete dissolution of 5.0 g of solid PMMA and 50 mg (1% w/w) of the [Ln(fluf)$_3$(L)] species in 100 mL of acetone with stirring at 60 °C for 1 h. Afterward, the solution was poured onto a Petri dish and heated at 60 °C, yielding a transparent polymeric film[30] after complete evaporation of the solvent.

2.2. Characterization Techniques

The elemental analyses were performed in a PerkinElmer CHN 2400 instrument. Fourier transform infrared (FTIR) spectra were measured using KBr pellets with a Bomem MB100 FTIR spectrometer from 550 to 4000 cm^{-1} with a spectral resolution of 4.0 cm^{-1}. Thermogravimetric (TG) analyses were performed in the 30−900 °C range on a Shimadzu equipment model TGA 60H under a nitrogen atmosphere of 100 $cm^3{\cdot}min^{-1}$ with a constant heating rate of 10 °C min^{-1}. The X-ray diffraction patterns were obtained with a Miniflex Rigaku

https://doi.org/10.1021/acsaom.2c00070
ACS Appl. Opt. Mater. 2023, 1, 354−366

diffractometer using Cu Kα1 radiation (30 kV and 15 mA) in the (2θ) 3−50° range and with 0.05 s of pass time. The diffuse reflectance data were recorded in the 250−800 spectral range with a Shimadzu UV-2600 equipment spectrophotometer containing an integrating sphere. $BaSO_4$ was used as the diffuse reflectance standard. The excitation and emission spectra of the Ln^{3+} complexes in solid state at room (~300 K) and liquid nitrogen (77 K) temperatures were recorded at an angle of 22.5° (front face) with a spectrofluorimeter (SPEX-Fluorolog 3) with a double grating between 0.5 and 2.0 mm monochromator (SPEX1680), and the excitation source was a 450 W xenon lamp. All spectra were recorded using a detector mode correction. Moreover, the luminescence decay curves of the emitting levels of the Ln^{3+} ion complexes were obtained at room temperature, using a phosphorimeter SPEX 1934D accessory coupled to the spectrofluorometer. The emission spectra of the $[Tb(fluf)_3(L)]$ complexes and the corresponding PMMA-doped films under sunlight irradiation were recorded using an Ocean Optics fiber optic (diameter 1 mm) connected to an Ocean Optics QE65000 spectrometer with a resolution up to 1 nm.

3. RESULTS AND DISCUSSION

The elemental analysis data of C, H, and N (Table S1) indicate the formation of complexes with the general formula $[Ln(fluf)_3(L)]$ where Ln^{3+}: Eu, Gd, and Tb and L: phen, tppo, topo, and dpso. The TG curves of the $[Ln(fluf)_3(L)]$ complexes were obtained in a $N_{2(g)}$ atmosphere in the 30−900 °C interval and revealed similar thermal events irrespective of the metal ions (Figures 2 and S1a−d) and corroborated the elemental analysis data and the stoichiometric ratio of 1:3:1 for the Ln^{3+}:fluf:L, respectively.

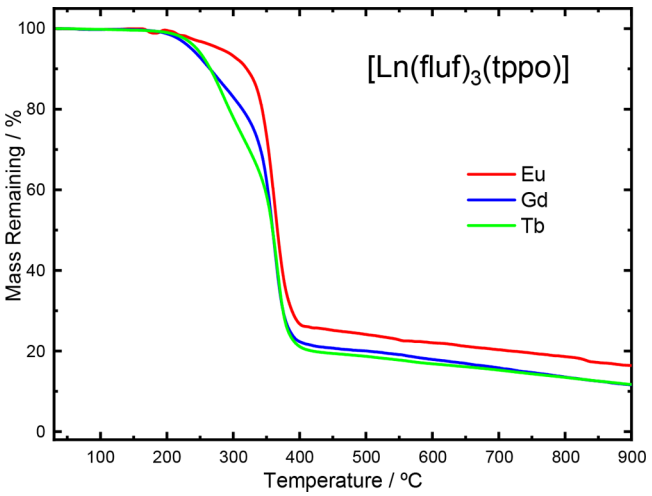

Figure 2. Thermogravimetric curves of the $[Ln(fluf)_3(tppo)]$ complexes, where Ln^{3+} stands for Eu, Gd, and Tb. The curves were obtained under a nitrogen atmosphere of 100 $cm^3 \cdot min^{-1}$ with a constant heating rate of 10 °C min^{-1} from 30 to 900 °C.

Also, the TG curves confirm that the compounds were obtained as anhydrous species and the $[Ln(fluf)_3(L)]$ complexes present thermal stability at around 200 °C. In general, the first event is the most significant and accounts for most of the mass loss that takes place in the 200−400 °C interval. In this thermal event occurs the decomposition of the organic moieties that continues in successive overlapped steps. We assume that the final product obtained at 900 °C, which is usually the respective lanthanide oxide, was not reached probably due to the nitrogen atmosphere. The TG curve profiles showed that the thermal behavior of the complexes is governed by the main fluf ligand.

FTIR spectra of the solid-state $[Ln(fluf)_3(L)]$ complexes, as well as the Nafluf the free Hfluf ligand are depicted in Figure S2a−d. The spectra revealed a narrow absorption band at around 3230−3320 cm^{-1} assigned to the N−H stretching mode (ν_{N-H}) from the fluf ligand. The ν_{N-H} mode of the complex compared with the free Hfluf shows a minimal shift, indicating that there is no coordination through the amine group as reported for other systems based on fenamates.[26,27,33] In addition, the absorption band corresponding to the carbonyl stretching mode of the free ligand (~1650 cm^{-1}) is absent in the $[Ln(fluf)_3(L)]$ complexes. On the other hand, two new absorption bands are observed in the intervals from 1605 to 1610 cm^{-1} and from 1390 to 1405 cm^{-1}, corresponding respectively to the asymmetric (ν_{as}) and symmetrical (ν_s) carbonyl modes.[26,27,33] Therefore, we can infer the effective coordination of the flufenamate ligand to the metal ion by the carboxylate group.

Additionally, the comparison between the $[Ln(fluf)_3(L)]$ complexes (Ln^{3+} = Eu, Gd, and Tb) and the corresponding sodium flufenamate salt allows the determination of the coordination mode adopted by the fluf ligand.[34] The difference between the ν_{as} and the ν_s modes ($\Delta\nu$) for the sodium salt and the complexes can be seen in Table S2. As one can see, the $\Delta\nu$ values for the complexes are slightly lower but close to the sodium salt, indicating that the fluf ligand coordinates to Ln^{3+} ions through a bidentate chelate coordination mode.[34] These results are corroborated with the FTIR data reported in previous reports.[27,33,35] The coordination of ancillary ligands to the Ln^{3+} ion was confirmed by the shift of the heteroaromatic C−N mode and the phosphine oxides ($\nu_{P=O}$) and sulfoxide ($\nu_{S=O}$) stretching modes to lower energies when compared with the free organic molecules,[36−38] as can be seen in Table S2.

The X-ray powder diffraction (XPD) patterns of the $[Ln(fluf)_3(L)]$ complexes (Figures 3a,b and S3a,b) reveal peaks with very low intensity and, in general, the highest intense one at angles around 5°, suggesting that the compounds present low crystallinity. A noticeable exception is the $[Ln(fluf)_3(phen)]$ species that present high crystallinity. Based on the diffraction pattern presented by the $[Ln(fluf)_3(phen)]$ complexes (Figure 3a), it is possible to infer that these compounds present isomorphic character among the three Eu^{3+}, Gd^{3+}, and Tb^{3+} compounds. The remarkable correspondence between the XRD and luminescence data concerning the phen and tppo species is significant, once the highly crystalline $[Eu(fluf)_3(phen)]$ complex (Figure 3a) presents well-defined Stark components even at room temperature, while the amorphous-like $[Eu(fluf)_3(tppo)]$ species (Figure 3b) reveal broader peaks arising from the Eu^{3+} ion intraconfigurational transitions.

4. PHOTOPHYSICAL PROPERTIES

4.1. Diffuse Reflectance Spectroscopy

The $[Eu(fluf)_3(L)]$ complexes are practically nonluminescent, different from the analogues Tb^{3+}-fluflenamates that show high green luminescence. Thus, in order to investigate the origin of such optical behavior, possibly related to the presence of ligand to metal charge transfer states, the diffuse reflectance spectra of the $[Ln(fluf)_3(L)]$ (Ln^{3+}: Eu, Gd, and Tb) complexes were

https://doi.org/10.1021/acsaom.2c00070
ACS Appl. Opt. Mater. 2023, 1, 354−366

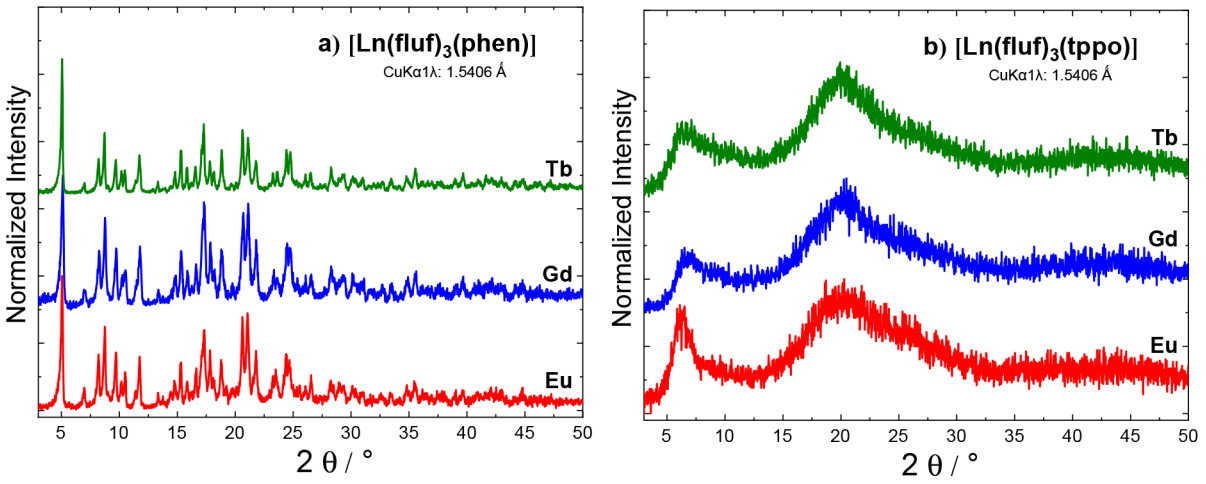

Figure 3. X-ray powder diffraction pattern (XPD) of the $[Ln(fluf)_3(L)]$ complexes where Ln: Eu^{3+} (red lines), Gd^{3+} (blue lines), and Tb^{3+} (green lines) and L: phen (a) and tppo (b) recorded at room temperature in the 3−50° range.

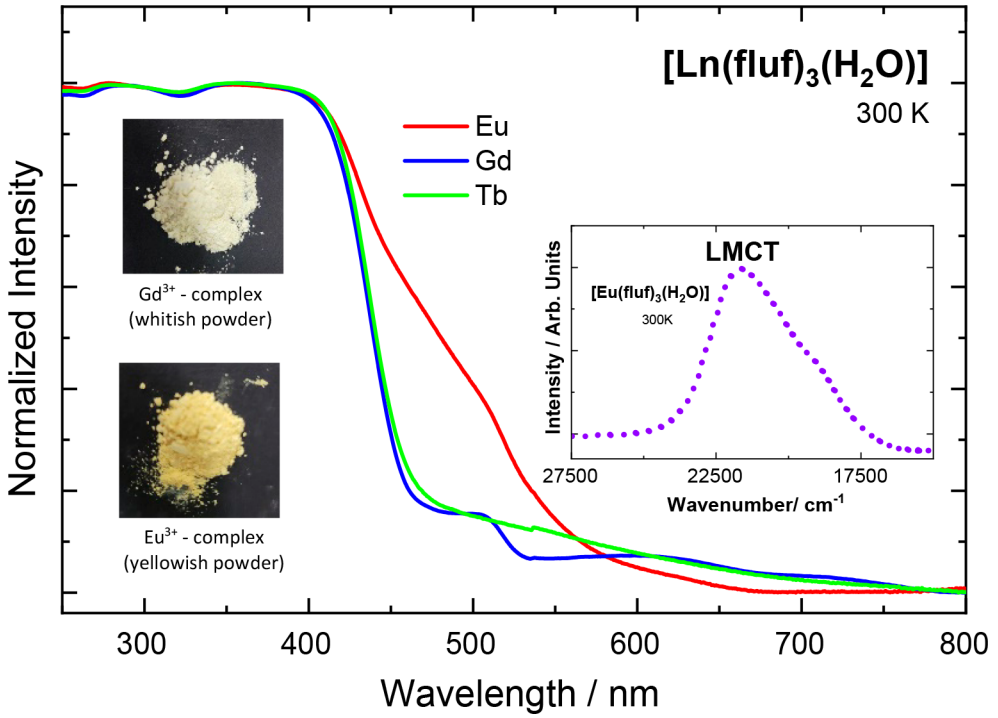

Figure 4. Diffuse reflectance spectra of the $[Ln(fluf)_3(H_2O)]$ compounds where Ln^{3+}: Eu (red line), Gd (blue line), and Tb (green line) were registered at 300 K. The inset figure shows the LMCT band (purple dotted curve) generated for the Eu^{3+} and Gd^{3+} complexes. The photographs correspond to the Eu^{3+} (yellowish powder) and Gd^{3+} flufenamates (whitish powder) under ambient light.

registered using $BaSO_4$ as a standard under room temperature in the 250−800 nm interval.

Once all the $[Eu(fluf)_3(L)]$ systems presented a similar spectral profile concerning the presence of the LMCT states, for the sake of clarity, Figure 4 shows the $[Ln(fluf)_3(H_2O)]$ diffuse reflectance spectra, as a representative of the whole series, as illustrated in Figure S4a−d for the other prepared complexes. The inset photographs were taken with a digital camera and show the influence of the LMCT band broadness (that extends to the visible region) on the absorption color of the Eu^{3+}-flufenamate, leading to a yellowish color, in contrast to the corresponding whitish Gd^{3+} compound. The intramolecular energy transfer process from the organic ligands to the europium ion will be discussed in section 4.4.

The inset plot in Figure 4 (purple dotted curve) presents the generated LMCT band for the aquo $[Eu(fluf)_3(H_2O)]$ complex. This plot was obtained by the arithmetic difference between the $[Eu(fluf)_3(H_2O)]$ and $[Gd(fluf)_3(H_2O)]$ diffuse reflectance spectra. Moreover, the LMCT bands obtained for all other complexes are illustrated in Figure S4a−d. Usually, the Gd^{3+} and Tb^{3+} compounds do not show the LMCT band at low energy.

4.2. Phosphorescent Behavior of $[Gd(fluf)_3(L)]$ Complexes

The Gd^{3+} ion is optically inactive above 315 nm due to the large energy gap between the $^8S_{7/2}$ ground state and the first $^6P_{7/2}$ excited state (32000 cm^{-1}),[25] which lies much higher than most of the organic ligand triplet states. In addition, the Gd^{3+} ion has an ionic radius similar to that of Eu^{3+} and Tb^{3+}

https://doi.org/10.1021/acsaom.2c00070
ACS Appl. Opt. Mater. 2023, 1, 354−366

ions and can mimic the chemical environment around the metal ion.[39,40]

Hence, the steady-state phosphorescence spectra of the solid-state [Gd(fluf)$_3$(L)] complexes (Figure 5) were recorded

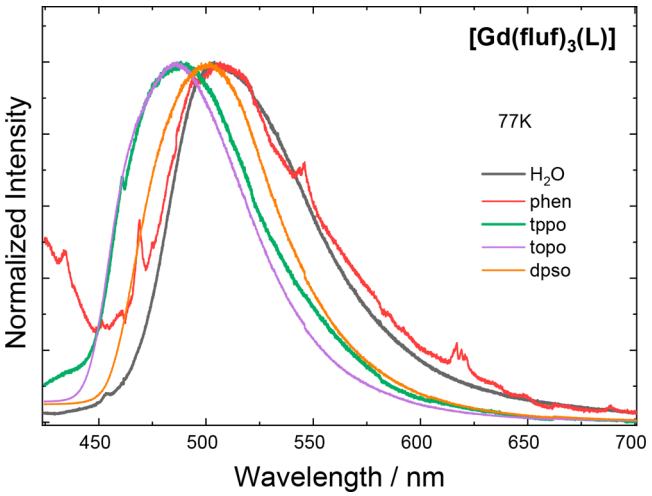

Figure 5. Phosphorescence spectra of the solid-state [Gd(fluf)$_3$(L)] complexes, where L: H_2O (black line), phen (red line), tppo (green line), topo (purple line), and dpso (orange line). The spectra were registered at 77 K from 425 to 700 nm with excitation in the maximum of the excitation spectra of each Gd^{3+}-flufenamates.

at 77 K in the 425−700 nm range. We assign the broad phosphorescence bands to the $T_1 \rightarrow S_0$ transition from the ligands (Table S3). It is worth mentioning that the narrow emission bands in the [Gd(fluf)$_3$(phen)] complex arise from 4f−4f transitions of the Eu^{3+} impurity.

4.3. Photoluminescent Investigation of [Tb(fluf)$_3$(L)] Complexes and PMMA-Doped Films

The excitation spectra of the [Tb(fluf)$_3$(L)] complexes (L: H_2O, phen, tppo, topo, dpso) and the doped PMMA films were monitored under excitation at 544 nm assigned to the $^5D_4 \rightarrow {}^7F_5$ transition of the Tb^{3+} ion in the 250−525 nm spectral range at 300 K (Figure 6a,b) and 77 K (Figure S5). The broad excitation bands are attributed to the $S_0 \rightarrow S_1$ intraligand transitions.[26,27] The comparison among these excitation spectra reveals interesting optical features: (i) the excitation bands for all PMMA:(1%)Tb(fluf)$_3$(L) systems are less broad than the corresponding complexes; (ii) the λ_{max} values of the $S_0 \rightarrow S_1$ transition for the doped films are blue-shifted compared with the complexes; (iii) the relative intensity of the organic moiety transitions in doped PMMA films is higher than those of the corresponding complexes.

The energy absorption in the polymer system is higher than that in the respective complexes because it is no longer possible to observe the $^7F_6 \rightarrow {}^5D_4$ transition of the Tb^{3+} ion (Figure 6a,b). Hence, the broad excitation bands in the doped PMMA materials show a more similar spectral profile than the complexes. This photoluminescent feature indicates that these luminescent materials are suitable for application under excitation at UVA, UVB, and UVC radiations. To the best of our knowledge, there is no study on Ln^{3+}-doped polymeric systems that have such noticeable features in this spectral range, including under sunlight exposure. Moreover, the low-temperature excitation spectra of the Tb^{3+} complexes are depicted in Figure S5 and reveal not too many broad bands with different spectral profiles. However, the complexes are still excitable at the wavelength of ∼405 nm, except for the complex containing topo as the ancillary ligand.

The emission spectra of the [Tb(fluf)$_3$(L)] complexes and the PMMA:(1%)Tb(fluf)$_3$(L) films were registered with excitation at 405 nm and under sunlight exposure at 300 K (Figure 7a−d). The corresponding low-temperature emission spectra of the [Tb(fluf)$_3$(L)] complexes (Figure S6) show similar profiles when compared with the room temperature ones; still, they present a higher resolution than those recorded at 300 K due to a decrease in the vibronic contributions.

4.3.1. UVA, UVB, and UVC Excitations. In general, the emission spectra of the Tb^{3+} complexes and doped polymer films at 300 K under excitation at 405, 310, and 254 nm correspond to UVA, UVB, and UVC, respectively (Figure 7b and Figure S7a,b). These spectra show the narrow emission bands assigned to intraconfigurational transitions $^5D_4 \rightarrow {}^7F_{6-0}$ of the Tb^{3+} ion at $^7F_6$ (489 nm), $^7F_5$ (544 nm), $^7F_4$ (585 nm), $^7F_3$ (621 nm), $^7F_2$ (646 nm), $^7F_1$ (667 nm), and $^7F_0$ (679 nm). It is noteworthy that the 4f−4f emission bands are broader in the PMMA polymer films than the corresponding Tb^{3+} complexes. As expected, the $^5D_4 \rightarrow {}^7F_5$ transition of the terbium ion shows the highest emission intensity in all of the complexes or doped films, which is responsible for the

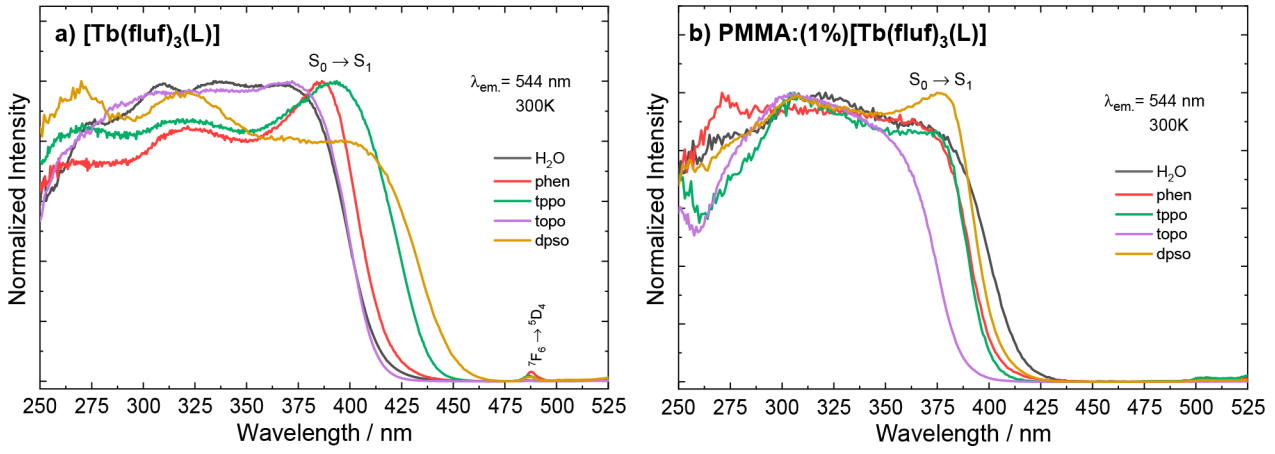

Figure 6. Excitation spectra of the solid-state [Tb(fluf)$_3$(L)] complexes (a) and PMMA:(1%)[Tb(fluf)$_3$(L)] (b) recorded at 300 K, monitoring the emission at the $^5D_4 \rightarrow {}^7F_5$ transition (λ_{em}: 544 nm) in the 250−525 nm range.

https://doi.org/10.1021/acsaom.2c00070
ACS Appl. Opt. Mater. 2023, 1, 354−366

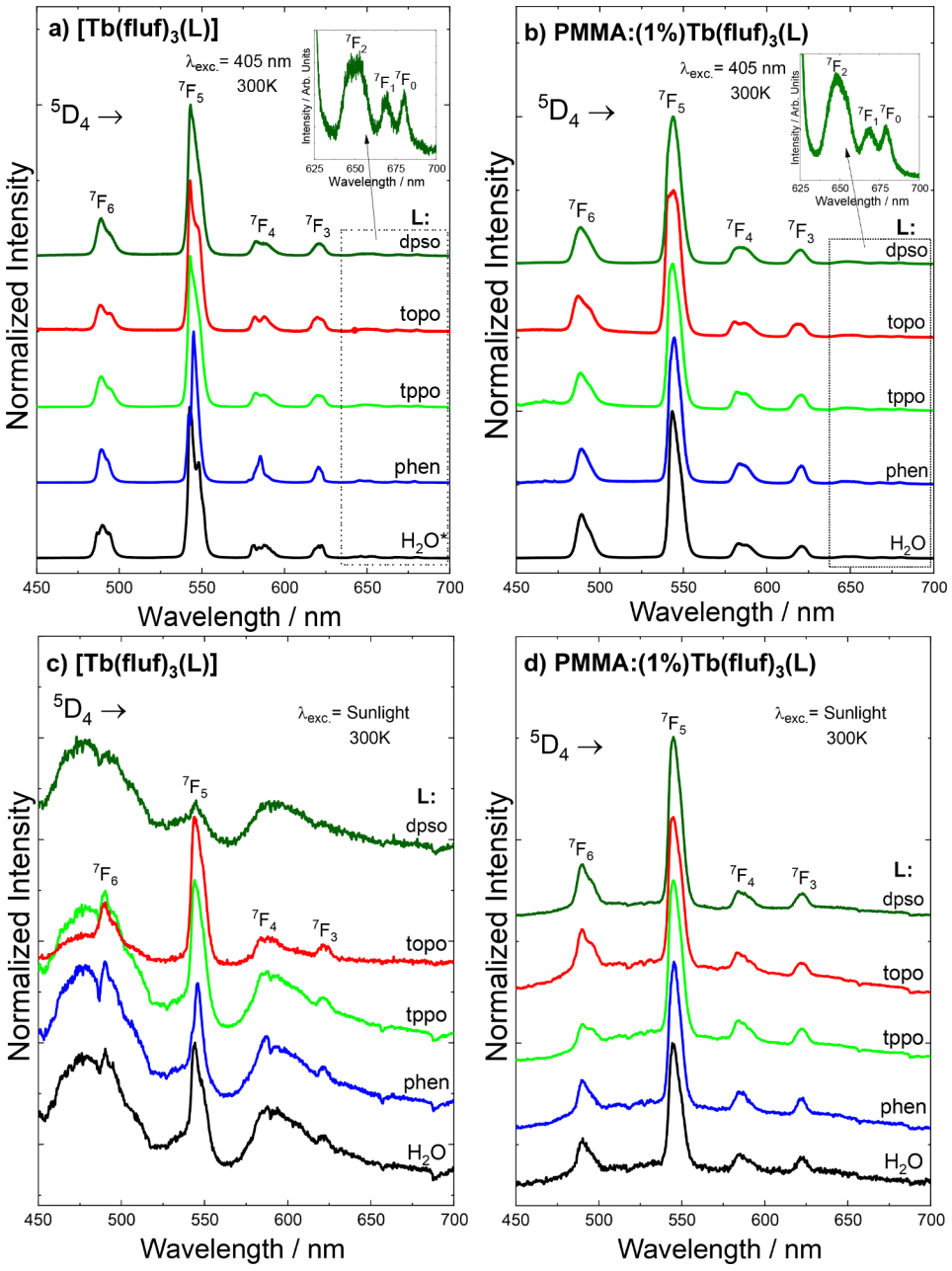

Figure 7. Emission spectra of the [Tb(fluf)$_3$(L)] complexes (a,c) and doped PMMA:(1%)[Tb(fluf)$_3$(L)] polymeric system (b,d) where L: H_2O*,[27] phen, tppo, topo, and dpso recorded at room temperature (300 K) under excitation at 405 nm (a,b) and sunlight (c,d) in the 450−700 nm range.

characteristic green color. At the same time, the $^5D_4 \rightarrow {}^7F_{2,1,0}$ transitions present the lowest intensity (inset Figure 7a,b). The absence of broad phosphorescence bands assigned to the $T_1 \rightarrow S_0$ transition of the organic moiety indicates an efficient ligand to metal transition (Figure 7b).

4.3.2. Sunlight Exposure. The emission spectra of doped polymer films recorded under sunlight exposure (Figure 7d) at 300 K also show spectral profiles assigned to $^5D_4 \rightarrow {}^7F_{6\text{-}0}$ transitions of the Tb^{3+} ion similar to those arising from the PMMA:(1%)Tb(fluf)$_3$(L) films (Figure 7b). In addition, Figure 7d shows a broad emission background band between 450 and 700 nm attributed to the sunlight excitation source that is overlapped with the $^5D_4 \rightarrow {}^7F_J$ transitions of the Tb^{3+} ion.

The emission spectra of the doped polymer films under sunlight exposure show the green emission color, arising from the $^5D_4 \rightarrow {}^7F_5$ (most intense) transition of the Tb^{3+} ion, similarly to those recorded under excitation wavelengths in the UVA, UVB, and UVC regions, as illustrated in Figures 7b and S7a,b, respectively. On the other hand, the emission spectral profiles of the Tb^{3+} complexes under sunlight exposure (Figure 7c) differ from those of doped polymeric films (Figure 7d), showing the high contribution of the sunlight background radiation. Thus, these optical results indicate that the PMMA:(1%)Tb(fluf)$_3$(L) polymeric films are versatile materials that can be used under different excitation sources such as sunlight radiation as well as UVA, UVB, and UVC. Therefore, these luminescent materials as efficient light-converting molecular devices and applied as LSCs.

https://doi.org/10.1021/acsaom.2c00070
ACS Appl. Opt. Mater. 2023, 1, 354−366

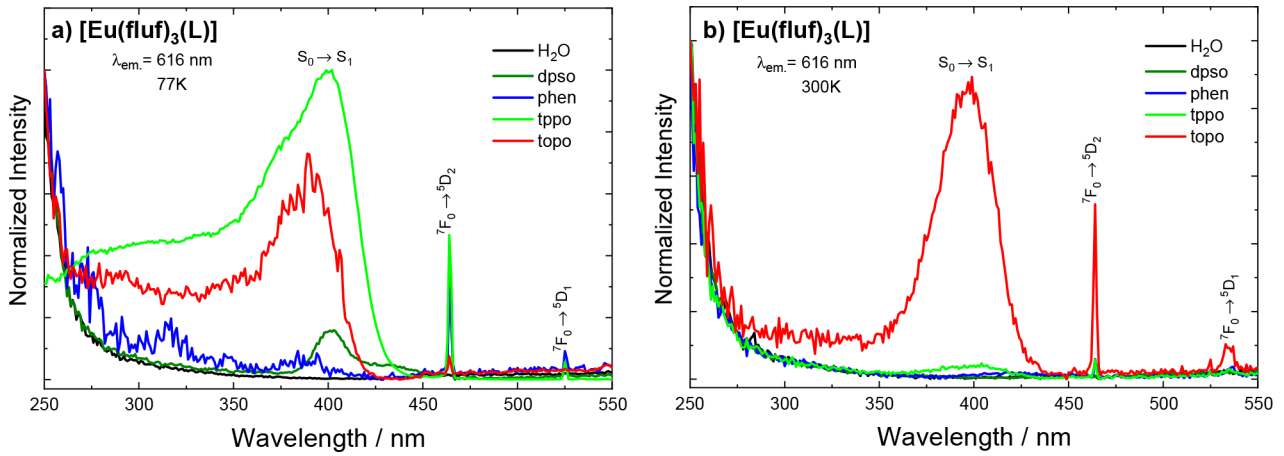

Figure 8. Excitation spectra of the solid-state $[Eu(fluf)_3(L)]$ complexes in the 250−575 nm range at 77 K (a) and room temperature (b) where L: H_2O, phen, tppo, topo, and dpso recorded the emission at the hypersensitive $^5D_0 \rightarrow {}^7F_2$ transition (λ_{em} = 616 nm).

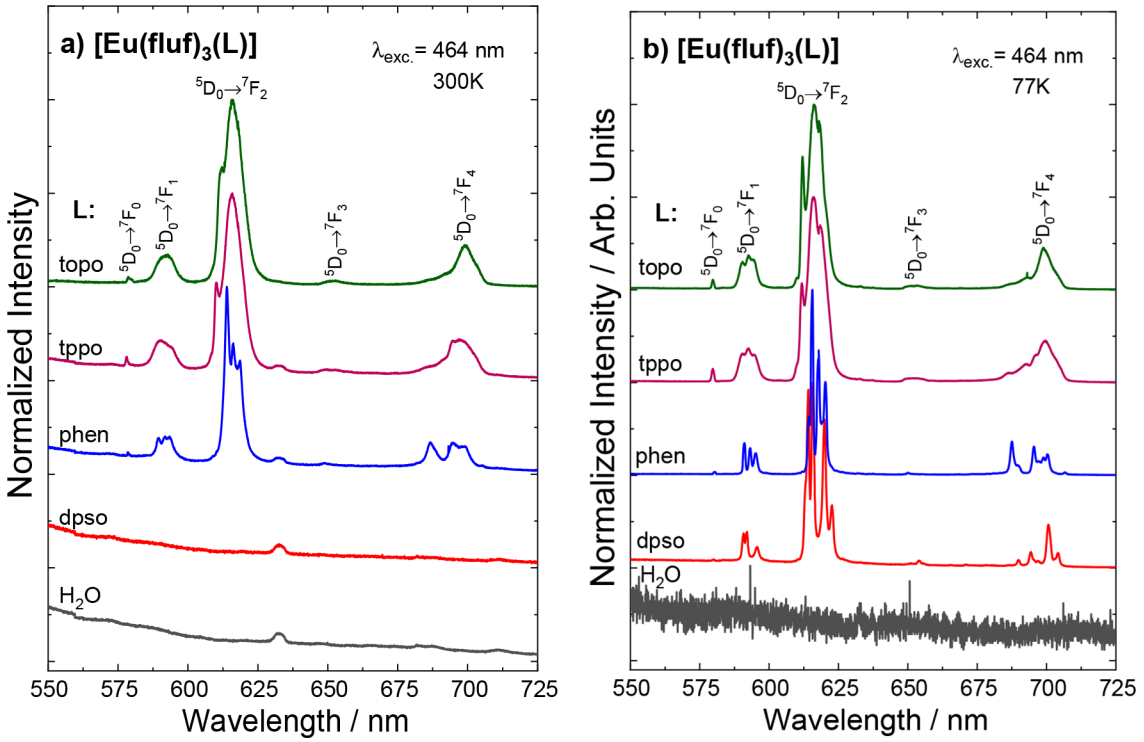

Figure 9. Emission spectra of the solid-state $[Eu(fluf)_3(L)]$ complexes at 300 K (a) and 77 K (b) where L: H_2O, dpso, phen, tppo, and topo were recorded with excitation at 464 nm in the range of 550−725 nm.

4.4. Photoluminescent Investigation of $[Eu(fluf)_3(L)]$ Complexes

Unlike Tb^{3+} complexes and doped polymer films, the Eu^{3+} equivalent systems are practically nonluminescent at room temperature. The excitation spectra of the $[Eu(fluf)_3(L)]$ coordination compounds were registered by monitoring the emission at the $^5D_0 \rightarrow {}^7F_2$ hypersensitive transition (~616 nm) of the Eu^{3+} ion at 77 and 300 K are depicted in Figure 8a,b, respectively. In general, the excitation spectra of the Eu^{3+} complexes recorded at low temperature (Figure 8a) show high-intensity broad excitation bands assigned to the $S_0 \rightarrow S_1$ transition centered on the organic moiety and the $^7F_0 \rightarrow {}^5D_{2,1}$ transitions of the Eu^{3+} ion at 464 and 525 nm, respectively. On the other hand, the room temperature excitation spectra of the $[Eu(fluf)_3(L)]$ complexes (Figure 8b) presented significantly lower intensity bands compared to those recorded at low temperature for the organic ligands or for metal ion transitions. However, the $[Eu(fluf)_3(topo)]$ complex is an exception showing a high-intensity broad excitation band attributed to the organic ligands. Moreover, it is also observed the narrow excitation peaks from $^7F_0 \rightarrow {}^5D_2$ and $^7F_0 \rightarrow {}^5D_1$ transitions of the Eu^{3+} ion. Interestingly, excitation spectra of the Tb^{3+} complexes (Figure 6a) present higher intensity center ligand bands than the Eu^{3+} analogue ones (Figure 8b), even at low temperature. These optical data suggest that the ligand to metal energy transfer in the Eu^{3+} compounds is operative, but both ligand and Eu^{3+} states are depopulated by the LMCT states.

The emission spectra of the $[Eu(fluf)_3(L)]$ complexes recorded at 300 and 77 K are depicted in Figure 9a,b,

https://doi.org/10.1021/acsaom.2c00070
ACS Appl. Opt. Mater. 2023, 1, 354−366

Table 1. Experimental Intensity Parameters ($\Omega_{2,4}$), Radiative (A_{rad}), and Nonradiative (A_{nrad}) Decay Rates, Emission Lifetime (τ_{464}), and Intrinsic Quantum Yield (Q_{Eu}^{Eu}) of the Solid-State [Eu(fluf)$_3$(L)] Complexes[a]

	[Eu(fluf)$_3$(L)]													
	$\Omega_2(10^{-20}$ cm^2)		$\Omega_4(10^{-20}$ cm^2)		$A_{rad}(s^{-1})$		$A_{nrad}(s^{-1})$		$A_{total}(s^{-1})$		τ (ms)		Q_{Eu}^{Eu} (%)	
L[b]	(300)	(77)	(300)	(77)	(300)	(77)	(300)	(77)	(300)	(77)	(300)	(77)	(300)	(77)
phen	12.7	12.9	7.6	6.7	548	562	10690	149	11240	711	0.089	1.407	5	79
tppo	11.8	11.5	5.5	6.3	485	487	1551	24	2037	511	0.491	1.955	15	92
topo	8.0	10.7	4.3	5.7	353	453	1647	202	2000	655	0.500	1.526	18	69
dpso		8.5		3.4		351		2442		2793		0.358		13

[a]L: phen, tppo, topo, and dpso. All data were determined at 300 and 77 K. [b]The spectroscopic data of the aquo Eu^{3+} complex were not determined due to the absence of emission bands.

respectively, and were recorded in the 525−725 nm range under excitation at 464 nm of the $^7F_0 \rightarrow {}^5D_2$ transition centered on the metal ion. The room temperature emission spectra (Figure 9a) revealed low intensity peaks arising from the $^5D_0 \rightarrow {}^7F_{0-4}$ transitions from the Eu^{3+} ion for all complexes. The most prominent peak corresponds to the $^5D_0 \rightarrow {}^7F_2$ transition at around 616 nm either at room or low temperature. It is noteworthy that for the [Eu(fluf)$_3$(L)] compounds with H_2O and dpso as ligands, none of the emission bands are observed. The presence of a single emission peak related to the $^5D_0 \rightarrow {}^7F_0$ transition (579 nm) indicates a rather low symmetry around the metal ion, belonging to C_{nv}, C_n, or C_s point groups.[41] Moreover, a large number of Stark components in the low-temperature spectra of the Eu^{3+}-flufenamates with phen and dpso ancillary ligands corroborate the low symmetry chemical environment around the metal ion.[42] Nevertheless, the 4f−4f transitions of the complexes containing the tppo and topo ancillary ligands present broader peaks than the other flufenamates even at 77 K. Such an experimental observation can be related to the higher amorphous-like character of the phosphinoxides-based Eu^{3+} compounds compared with the rest of the series, corroborating the XPD data.

Interestingly, the low-temperature Eu^{3+}-flufenamate emission spectra (Figure 9b) differ from the room temperature analogue by presenting better spectral resolution due to fewer vibronic contributions for the majority of the [Eu(fluf)$_3$(L)] species. However, the 4f−4f bands in the 77 K spectra are more intense than at room temperature, suggesting that the role of the LMCT states is temperature-dependent as already observed for other systems.[42−44] Such an observation is remarkable for the [Eu(fluf)$_3$(dpso)] complex, for which at room temperature only a vibronic transition at 633 nm can be observed, while in lowering the temperature, the intraconfigurational $^5D_0 \rightarrow {}^7F_{0-4}$ transitions become as intense as any of the other Eu^{3+}-flufenamates, except for the aquo Eu^{3+} complex. Moreover, it is observed (especially in the 77 K spectra) that the spectral profile of each [Eu(fluf)$_3$(L)] are significantly different between each other, suggesting that the chemical environment around the Eu^{3+} ion is deeply affected by the ancillary ligands coordinated to the metal ion.

The strong luminescence quenching through the LMCT state is highly dependent on the energy position of the T_1 state of the organic ligand or $^5D_0$ and $^5D_1$ levels of the Eu^{3+} ion.[23,45] Likewise, the LMCT quenching process is also thermally activated, showing the dependence of the temperature on the lifetimes of the emitting $^5D_0$ level (Table 1).[46]

Spectral features like bandwidth and λ_{max} are dependent on the nature of the ancillary ligand, but in general, the bands are rather broad and vary between 28000 and 16000 cm^{-1} with maxima in the 24400 to 20400 cm^{-1} range.

The experimental intensity parameter (Ω_2 and Ω_4) values were calculated for the Eu^{3+} complexes according to eq 1:

$$A_{0\rightarrow\lambda} = \frac{4\omega^3 e^2 \chi}{3\hbar c^3}\Omega_\lambda |\langle {}^5D_0 \| U^{(\lambda)} \| {}^7F_\lambda\rangle|^2 \quad (1)$$

in which ω is the angular frequency of the transition, e is the elementary charge, χ is the Lorentz local field correction factor, $\hbar$ is the reduced Planck's constant, and c is the speed of light. The quantity $|\langle {}^5D_0 \| U^{(\lambda)} \| {}^7F_\lambda\rangle|^2$ is the squared reduced matrix elements whose values are equal to 0.0032 and 0.0023 for $\lambda = 2$ and 4, respectively.[47,48] The χ values have been calculated using the index of refraction $n = 1.5$.[24] Recent studies revealed that the Ω_2 values are by far more sensitive to even small angular variations, while the Ω_4 values are sensitive to both angular and ligating atom−Eu^{3+} ion distance variations.[49,50]

The experimental values for the spontaneous emission coefficients ($A_{0\rightarrow J}$) related to the $^5D_0 \rightarrow {}^7F_{0-4}$ transitions of the Eu^{3+} ion were determined from the emission spectra of the [Eu(fluf)$_3$(L)] species by eq 2:[13,28,48]

$$A_{0\rightarrow J} = \left(\frac{S_{0\rightarrow J}}{S_{0\rightarrow 1}}\right) A_{0\rightarrow 1} \quad (2)$$

where $S_{0\rightarrow 1}$ and $S_{0\rightarrow J}$ correspond to the areas under the emission curves of the $^5D_0 \rightarrow {}^7F_1$ and $^5D_0 \rightarrow {}^7F_{2,4,6}$, respectively, although the $^5D_0 \rightarrow {}^7F_6$ is often not experimentally observed.[28] Additionally, the $^5D_0 \rightarrow {}^7F_1$ transition is almost completely governed by the magnetic dipole (MD) mechanism, and its intensity is practically insensitive ($n = 1.5$, $A_{0\rightarrow 1} \sim 50$ s^{-1})[28] to the point symmetry chemical environment around the Eu^{3+} ion, thus, this transition can be used as an internal reference to determine the $A_{0\rightarrow J}$ values.

The intrinsic emission quantum yield (Q_{Eu}^{Eu})[28,51] is defined as the ratio between the radiative (A_{rad}) and the total (A_{total}) decay rates that are given by the sum of radiative and nonradiative (A_{nrad}) rates (eq 3). Moreover, there is a relationship between A_{total} rate and the emitting level lifetime (τ_{obs}) given by eq 4[51] in which the τ_{obs} values were calculated from the luminescence decay curves excited at the $^7F_0 \rightarrow {}^5D_2$ transition (~464 nm) and registered at room temperature (Figure S8a) and 77 K (Figure S8b).

$$Q_{Eu}^{Eu} = \frac{A_{rad}}{A_{rad} + A_{nrad}} = \frac{\tau_{obs}}{\tau_{rad}} \quad (3)$$

$$\tau_{464} = \frac{1}{A_{rad} + A_{nrad}} = \frac{1}{A_{total}} \quad (4)$$

https://doi.org/10.1021/acsaom.2c00070
ACS Appl. Opt. Mater. 2023, 1, 354−366

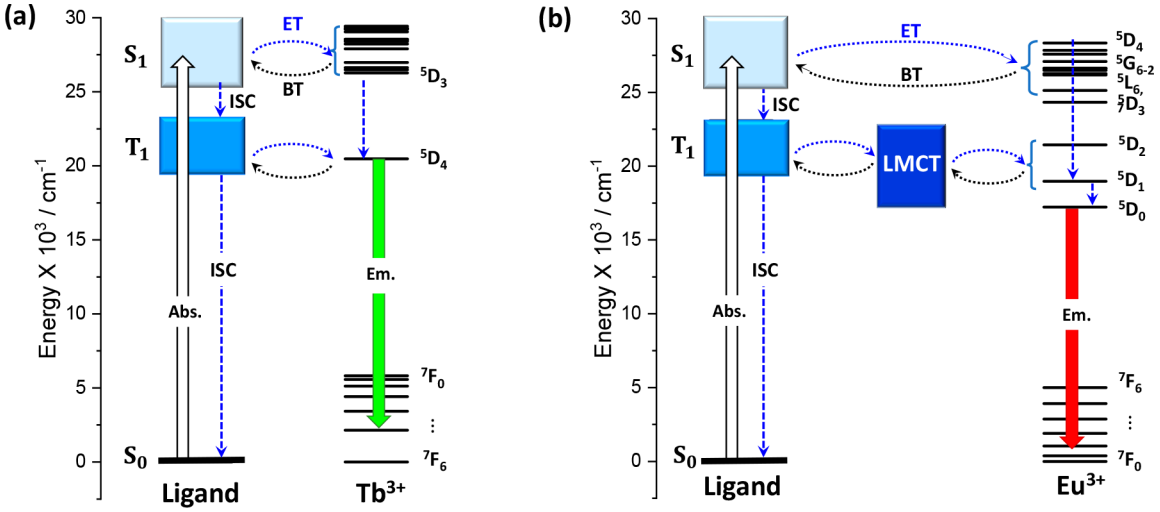

Figure 10. Partial energy level diagram of the $[Ln(fluf)_3(L)]$ complexes with (a) Tb^{3+} ion and (b) Eu^{3+} ion. The emission arises from $^5D_4$ and $^5D_0$ emitting levels, respectively. S_0 and S_1 are the ligand ground and lowest singlet excited states, respectively. T_1 is the lowest triplet ligand level, Abs. is the initial absorption, ISC is the intersystem crossing, Em. is the emission. ET and BT are the forward and backward energy transfer rates, respectively.

It is noteworthy to mention that the A_{rad} values might present temperature dependence, while there are several factors that can increase the A_{nrad} such as vibronic coupling with organic groups like C−H, N−H, and O−H.[28,52] The luminescence decay curves were obtained monitoring the emission at the $^5D_0 \rightarrow {}^7F_2$ transition (616 nm) and with excitation at the $^7F_0 \rightarrow {}^5D_2$ transition (464 nm) of the Eu^{3+} ion.

The values of the Ω_2 and Ω_4 parameters of the $[Eu(fluf)_3(L)]$ (L: phen, tppo, topo, and dpso) were obtained at 300 and 77 K (Table 1). These experimental parameters were not calculated to the aquo and dpso complexes at room temperature due to the presence of LMCT band at lower energy. The low Ω_2 values obtained at different temperatures indicate small angular variations of the Eu^{3+} coordination geometry due to the low emission intensity of the hypersensitive $^5D_0 \rightarrow {}^7F_2$ transition. In addition, the Ω_2 values are similar at the same temperature. The Ω_2 parameters at 77 K are slightly higher than those at 300 K, suggesting a higher angular variation in the coordination geometry around the europium ion at low temperature.

The Ω_4 parameter values present very similar values, indicating, to similar bond distances between the metal ion and the ligating atoms from the ligands. When we compare the Ω_4 parameter values of the flufenamate systems with other Eu^{3+} carboxylate complexes[22,53] obtained at room temperature, the former present lower values, indicating a less sensitivity to the distances and, therefore, to covalency effects.[24,49] This behavior is probably due to variations in the distance between a ligating Eu^{3+} atom, though angular variation in the first coordination sphere may also contribute to this very fact.

The systematic increase in both $\Omega_{2,4}$ values points to a structural change around the metal ion that, consequently, affects the relative position of the LMCT state and the efficiency of the energy transfer process. Such experimental data support the increase in the luminescence intensity at a lower temperature compared with the room temperature values.

In general, the A_{rad} values for the $[Eu(fluf)_3(L)]$ complexes obtained at room and low temperature show a small difference (Table 1), indicating that the radiative rate contributions are almost insensitive to the temperature changes. On the other hand, the A_{nrad} values are hugely decreased from 300 to 77 K, which are associated with a lowering of the LMCT band position and multiphonon relaxation contributions at low temperature, increasing luminescence intensity. However, this optical feature is not observed for the aquo Eu^{3+} complex due to the contributions of both effects, LMCT and multiphonon relaxation. Table 1 shows an increase in the τ values as the temperature is lowered, suggesting that the LMCT state is operative in the luminescence quenching process of the Eu^{3+} complexes.[42]

The intrinsic quantum yields (Q_{Eu}^{Eu}) values of the $[Eu(fluf)_3(L)]$ complexes obtained at room temperature are small (3 and 18%). On the other hand, the Q_{Eu}^{Eu} values recorded at low temperature show a significant increase (66−92%) due to the decrease of the A_{nrad} rate, arising mainly from the lower LMCT contributions as a suppressing channel (Table 1). In addition, it was impossible to determine the intrinsic quantum yield for the complexes containing H_2O and dpso ligand due to the absence of emission bands at 300 K.

4.4.1. Intramolecular Energy Transfer. Based on the spectroscopic data of the Ln^{3+} complexes (Ln^{3+}: Eu and Tb), the energy level diagrams for the Tb^{3+} (Figure 10a) and Eu^{3+} (Figure 10b) compounds were built to elucidate their intramolecular energy transfer pathways. The incoming radiation is first absorbed by the organic ligands that are excited from a fundamental singlet (S_0) to a first excited (S_1) state. Subsequently, the energy is nonradiatively transferred through intersystem crossing (ISC) to an excited triplet (T_1) level (Figure 10a,b), from which the energy transfer to Eu^{3+} and Tb^{3+} ions is entirely different.

The partial energy level diagram for the Tb^{3+} complexes (Figure 10a) indicates that the high luminescence intensity of the $[Tb(fluf)_3(L)]$ complexes (L: H_2O, phen, tppo, topo, and dpso) can be attributed to the suitable energy gap between ligand-centered T_1 states and the main energy level of the Tb^{3+} ion ($^5D_4$), i.e., $\Delta E \sim 4080$ cm^{-1}, that is beyond the optimum value of $\Delta E \sim 2000$ cm^{-1} to avoid as much as possible the energy back-transfer (BT) and the consequent efficiency loss.[54] This experimental value is rather similar to those reported in

https://doi.org/10.1021/acsaom.2c00070
ACS Appl. Opt. Mater. 2023, 1, 354−366

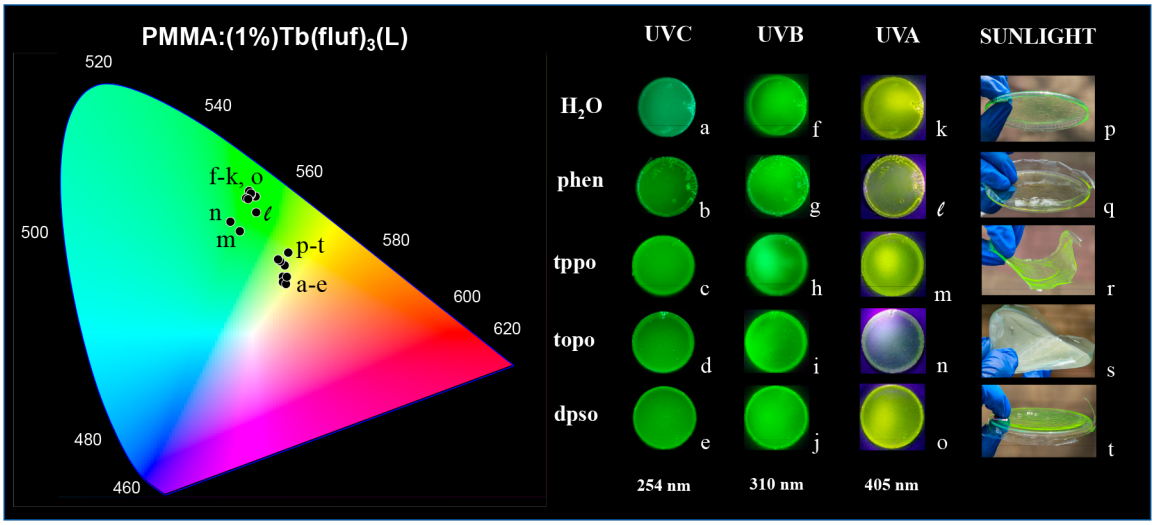

Figure 11. CIE diagram for the doped PMMA:1%Tb(fluf)$_3$(L) films (L: H_2O, phen, tppo, topo, and dpso) obtained from their emission spectra at 254 nm (a–e), 310 nm (f–j), 405 nm (k–o), and under sunlight exposure (p–t). All spectra were registered at room temperature. The inset figures are photographs of polymeric films taken with a digital camera exhibiting their green emission color under different wavelength irradiation. The photographs from p–t (sunlight irradiation) were taken at an open external environment which allows the direct exposure and excitation of films.

the literature[26,27] and reveals a remarkable independence of T_1 energy values on the ancillary ligands.

On the other hand, the intramolecular energy transfer pathways (Figure 10b) involve the significant overlapping of the LMCT band with the Eu^{3+} excited levels as $^5D_3$ (24300 cm^{-1}), $^5D_2$ (21400 cm^{-1}), $^5D_1$ (18970 cm^{-1}), and $^5D_0$ (17230 cm^{-1}).[41] This spectroscopic behavior shows that the energy back-transfer pathways from these energy levels to the LMCT state leads to a strong luminescence quenching of the metal ion. Thus, it is possible to infer that the LMCT states play a crucial role in the quenching process by depopulating both the organic ligand states and the energy levels of the Eu^{3+} ion.[23] The low energy of the LMCT state in the [Eu(fluf)$_3$(L)] complexes can also be rationalized considering that the carboxylate group and both phenyl rings and the bridging amino group are all coplanar.[55−59] Thus, once the nitrogen atom is nearly sp^2-hybridized,[60] the lone pair in the p-orbital participates in the conjugation via the π-electron system that is formed by the aromatic rings and increases the electron density that is shifted toward the COO^- group. Consequently, the LMCT state can be placed at lower energies.[42]

The coordinates in the CIE (Commission Internationale l'Eclairage) chromaticity diagrams were determined based on the emission spectra of the doped PMMA:(1%)Tb(fluf)$_3$(L) films under excitation at 254 nm (UVC), 310 nm (UVB), and 405 nm (UVA), as well as under sunlight exposure (Figure 11). All *x*,*y* coordinates for the doped polymer films excited at UVB and UVC are in the green region, while for those excited UVA, the coordinates are shifted toward the yellow region. while those irradiated at 254 nm present a more centered distribution in the CIE diagram. When the polymer films are irradiated by sunlight in an open and external environment, the points are shifted toward the center of the diagram (Figure 11) due to the contribution of the solar radiation background emission.

5. CONCLUSION

The [Ln(fluf)$_3$(L)] complexes (Ln^{3+}: Eu and Tb) (L: H_2O, phen, tppo, topo, and dpso) doped into a PMMA matrix in a mass concentration of 1% were successfully synthesized. The complexes are thermostable at around 200 °C, and the XPD data indicate that all of the complexes are amorphous-like, except for that containing the phen ligand.

The [Eu(fluf)$_3$(L)] complexes reveal an almost complete absence of luminescence at room temperature due to an operative luminescence quenching due to the presence of the LMCT state. Moreover, the photoluminescent properties of this system show a strong dependence of the LMCT state as a function of the temperature. The intrinsic emission quantum efficiency (Q_{Eu}^{Eu}) of the [Eu(fluf)$_3$(L)] are deeply affected by the temperature due to the LMCT contributions, increasing at lower temperatures.

The photophysical investigation reveals that the doped PMMA:1%Tb(fluf)$_3$(L) films exhibit high emission intensity under excitation at UVA, UVB, and UVC regions, arising from the $^5D_4 \rightarrow {}^7F_{6-0}$ transitions of the Tb^{3+} ion. The doped polymer films show green emission color when excited by sunlight radiation at an open external environment.

Finally, the photoluminescent results point out that the Tb^{3+}-doped polymeric films are versatile photonic materials that can be used under different excitation sources with UVA, UVB, and UVC radiation and even at sunlight exposure. Therefore, these luminescent polymer materials can act as efficient light-converting molecular devices and can be applied as luminescent solar concentrators.

■ ASSOCIATED CONTENT

Supporting Information

The Supporting Information is available free of charge at https://pubs.acs.org/doi/10.1021/acsaom.2c00070.

Elemental analysis table, characterization techniques, low temperature measurements, and supporting figures (PDF)

https://doi.org/10.1021/acsaom.2c00070
ACS Appl. Opt. Mater. 2023, 1, 354−366

AUTHOR INFORMATION

Corresponding Authors

Israel P. Assunção − *Department of Fundamental Chemistry, Institute of Chemistry, University of São Paulo, São Paulo, SP 05508-000, Brazil; Education, Science and Technology, Federal Institute of São Paulo, São Paulo 01109-010, Brazil;* orcid.org/0000-0003-0438-0787; Email: ipassunc@iq.usp.br

Hermi F. Brito − *Department of Fundamental Chemistry, Institute of Chemistry, University of São Paulo, São Paulo, SP 05508-000, Brazil*; Email: hefbrito@iq.usp.br

Authors

Israel F. Costa − *Department of Fundamental Chemistry, Institute of Chemistry, University of São Paulo, São Paulo, SP 05508-000, Brazil;* orcid.org/0000-0002-4829-0663

Paulo R. S. Santos − *Department of Chemistry, Federal University of Paraíba, João Pessoa, PB 58051-970, Brazil*

Ercules E. S. Teotonio − *Department of Chemistry, Federal University of Paraíba, João Pessoa, PB 58051-970, Brazil; Institute of Inorganic Chemistry, Christian-Albrechts University of Kiel, 24118 Kiel, Germany;* orcid.org/0000-0003-0184-0645

Maria Claudia F. C. Felinto − *Nuclear and Energy Research Institute − IPEN/CNEN, São Paulo, SP 05508-000, Brazil*

Ulrich Kynast − *Institute for Optical Technologies, Muenster University of Applied Sciences, 48565 Steinfurt, Germany;* orcid.org/0000-0002-8796-2282

Wagner M. Faustino − *Department of Chemistry, Federal University of Paraíba, João Pessoa, PB 58051-970, Brazil*

Oscar Malta − *Department of Fundamental Chemistry, Federal University of Pernambuco, Recife, PE 50670-901, Brazil*

Complete contact information is available at: https://pubs.acs.org/10.1021/acsaom.2c00070

Author Contributions

I. P. Assunção: Conceptualization, methodology, investigation, data curation, writing of the original draft, visualization. I. F. Costa: Methodology, investigation, data curation, writing of the original draft. P. R. S. Santos: Methodology, investigation. E. E. S. Teotônio: Conceptualization, writing of the original draft. M. C. F. C. Felinto: Conceptualization, writing of the original draft. U. Kynast: Conceptualization, writing of the original draft. W. M. Faustino: Conceptualization, writing of the original draft. O. L. Malta: Conceptualization, investigation, writing of the original draft, visualization, supervision. H. F. Brito: Conceptualization, investigation, data curation, writing of the original draft, visualization, supervision.

Notes

The authors declare no competing financial interest.

ACKNOWLEDGMENTS

The authors are grateful to the Brazilian funding agencies CNPq and FAPESP for financial support and to the photographer Cezar Guizzo for the polymeric films' photographs. Hermi F. Brito is grateful to CNPq for the research grant (306951/2018-5).

REFERENCES

(1) Debije, M. G.; Verbunt, P. P. C. Thirty Years of Luminescent Solar Concentrator Research: Solar Energy for the Built Environment. *Adv. Energy Mater.* **2012**, *2* (1), 12−35.

(2) Batchelder, J. S.; Zewai, A. H.; Cole, T. Luminescent Solar Concentrators 1: Theory of Operation and Techniques for Performance Evaluation. *Appl. Opt.* **1979**, *18* (18), 3090.

(3) Weber, W. H.; Lambe, J. Luminescent Greenhouse Collector for Solar Radiation. *Appl. Opt.* **1976**, *15* (10), 2299−2300.

(4) Eliseeva, S.; Bünzli, J. C. G. Lanthanide Luminescence for Functional Materials and Bio-Sciences. *Chem. Soc. Rev.* **2010**, *39* (1), 189−227.

(5) Gupta, B. K.; Haranath, D.; Saini, S.; Singh, V. N.; Shanker, V. Synthesis and Characterization of Ultra-Fine Y_2O_3:Eu^{3+} Nanophosphors for Luminescent Security Ink Applications. *Nanotechnology* **2010**, *21* (5), 055607.

(6) Bünzli, J. C. G. Lanthanide Light for Biology and Medical Diagnosis. *J. Lumin.* **2016**, *170*, 866−878.

(7) Ilmi, R.; Iftikhar, K. Photophysical properties of Lanthanide(III) 1,1,1-trifluoro-2,4-pentanedione complexes with 2,2′-Bipyridyl: An experimental and theoretical investigation. *J. Photochem. Photobiol. A: Chem.* **2017**, *333*, 142−155.

(8) Guimarães, L. B.; Botas, A. M. P.; Felinto, M. C. F. C.; Ferreira, R. A. S.; Carlos, L. D.; Malta, O. L.; Brito, H. F. Highly Sensitive and Precise Optical Temperature Sensors Based on New Luminescent Tb^{3+}/Eu^{3+} tetrakis Complexes with Imidazolic Counterions. *Mater. Adv.* **2020**, *1* (6), 1988−1995.

(9) Savchuk, O. A.; Carvajal, J. J.; Brites, C. D. S.; Carlos, L. D.; Aguilo, M.; Diaz, F. Upconversion Thermometry: A New Tool to Measure the Thermal Resistance of Nanoparticles. *Nanoscale* **2018**, *10* (14), 6602−6610.

(10) Francisco, L. H. C.; Felinto, M. C. F. C.; Brito, H. F.; Teotonio, E. E. S; Malta, O. L. Development of Highly Luminescent PMMA Films Doped with Eu^{3+} β-Diketonate Coordinated on Ancillary Ligand. *J. Mater. Sci. Mater. Electron.* **2019**, *30* (18), 16922−16931.

(11) Gil-kowalczyk, M.; Łyszczek, R.; Jusza, A.; Piramidowicz, R. Thermal, Spectroscopy and Luminescent Characterization of Hybrid PMMA/Lanthanide Complex Materials. *Materials* **2021**, *14* (12), 3156.

(12) Ferreira, R. A. S.; Correia, S. F. H.; Monguzzi, A.; Liu, X.; Meinardi, F. Spectral Converters for Photovoltaics − What's Ahead. *Mater. Today* **2020**, *33*, 105−121.

(13) de Sá, G. F.; Malta, O. L.; Donega, C. D. M.; Simas, A. M.; Longo, R. L.; Santa-Cruz, P. A.; da Silva, E. F., Jr. Spectroscopic Properties and Design of Highly Luminescent Lanthanide Coordination Complexes. *Coord. Chem. Rev.* **2000**, *196* (1), 165−195.

(14) Malta, O. Ligand—Rare-Earth Ion Energy Transfer in Coordination Compounds. A Theoretical Approach. *J. Lumin.* **1997**, *71* (3), 229−236.

(15) Buono-core, G. E.; Li, H.; Marciniak, B. Quenching of Excited States by Lanthanide Ions and Chelates in Solution. *Coord. Chem. Rev.* **1990**, *99*, 55−87.

(16) Faustino, W. M.; Malta, O. L.; de Sa, G. F. Intramolecular Energy Transfer through Charge Transfer State in Lanthanide Compounds : A Theoretical Approach. *J. Chem. Phys.* **2005**, *122* (5), 054109.

(17) Crosby, G. A.; Whan, R. E.; Freeman, J. J. Spectroscopic Studies of Rare Earth Chelates. *J. Phys. Chem.* **1962**, *66* (12), 2493−2499.

(18) Whan, R. E.; Crosby, G. A. Luminescence Studies of Rare Earth Complexes: Benzoylacetonate and Dibenzoylmethide Chelates. *J. Mol. Spectrosc.* **1962**, *8* (1−6), 315−327.

(19) Carrington, A.; dos Santos-Veiga, J. Electron Spin Resonance Spectra of Nitrogen Heterocyclic Radical Ions. *Mol. Phys.* **1962**, *5*, 21−29.

(20) Jørgensen, C. K.; Meriläinen, P.; Lukkari, S.; Block-Bolten, A.; Toguri, J. M.; Flood, H. New Theory for the Electron Transfer Spectra of Acetylacetonate Complexes. *Acta Chem. Scand.* **1962**, *16*, 2406−2410.

(21) Miranda, Y. C.; Pereira, L. L. A. L.; Barbosa, J. H. P.; Brito, H. F.; Felinto, M. C. F. C.; Malta, O. L.; Faustino, W. M.; Teotonio, E. E. S. The Role of the Ligand-to-Metal Charge-Transfer State in the Dipivaloylmethanate-Lanthanide Intramolecular Energy Transfer Process. *Eur. J. Inorg. Chem.* **2015**, *2015* (18), 3019−3027.
(22) Assuncao, I. P.; Carneiro Neto, A. N.; Moura, R. T.; Pedroso, C. C. S.; Silva, I. G. N.; Felinto, M. C. F. C.; Teotonio, E. E. S.; Malta, O. L.; Brito, H. F. Odd-Even Effect on Luminescence Properties of Europium Aliphatic Dicarboxylate Complexes. *ChemPhysChem.* **2019**, *20* (15), 1931−1940.
(23) Faustino, W. M.; Malta, O. L.; Teotonio, E. E. S.; Brito, H. F.; Simas, A. M.; de Sá, G. F. Photoluminescence of Europium(III) Dithiocarbamate Complexes: Electronic Structure, Charge Transfer and Energy Transfer. *J. Phys. Chem. A* **2006**, *110* (7), 2510−2516.
(24) Carneiro Neto, A. N.; Teotonio, E. E. S.; de Sá, G. F.; Brito, H. F.; Legendziewicz, J.; Carlos, L. D.; Felinto, M. C. F. C.; Gawryszewska, P.; Moura, R. T.; Longo, R. L.; Faustino, W. M.; Malta, O. L. Modeling Intramolecular Energy Transfer in Lanthanide Chelates: A Critical Review and Recent Advances. *Handb. Phys. Chem. Rare Earths* **2019**, *56*, 55−162.
(25) Carnall, W. T.; Crosswhite, H.; Crosswhite, H. M. Energy Level Structure and Transition Probabilities in the Spectra of the trivlent Lanthanides in LaF_3. *J. Chem. Phys.* **1989**, *90*, 3443−3457.
(26) Assunção, I. P.; Bredol, M.; Kasprzycka, E.; Kynast, U. H.; Lezhnina, M. Near-UV-Excitable, Green-Emitting Tb^{3+}-Based Complexes. *Inorg. Chim. Acta* **2021**, *515* (August 2020), 120071.
(27) Kasprzycka, E.; Assunção, I. P.; Bredol, M.; Lezhnina, M.; Kynast, U. H. Preparation, Characterization and Optical Properties of Rare Earth Complexes with Derivatives of N-Phenylanthranilic Acid. *J. Lumin.* **2021**, *232*, 117818.
(28) Brito, H. F.; Malta, O. L.; Felinto, M. C. F. C.; Teotônio, E. E. S.*Luminescence Phenomena Involving Metal Enolates*; John Wiley & Sons, Ltd., 2009; pp 131−184.
(29) Binnemans, K. Rare-Earth Beta-Diketonates. *Handb. Phys. Chem. Rare Earths* **2005**, *35*, 107−272.
(30) Kai, J.; Felinto, M. C. F. C.; Nunes, L. A. O.; Malta, O. L.; Brito, H. F. Intermolecular Energy Transfer and Photostability of Luminescence-Tuneable Multicolour PMMA Films Doped with Lanthanide−β-Diketonate Complexes. *J. Mater. Chem.* **2011**, *21* (11), 3796−3802.
(31) Bünzli, J. C. G. On the Design of Highly Luminescent Lanthanide Complexes. *Coord. Chem. Rev.* **2015**, *293*−*294*, 19−47.
(32) Brito, H. F.; Malta, O. L.; Alves de Carvalho, C. A.; Menezes, J. F. S.; Souza, L. R.; Ferraz, R. Luminescence Behavior of Eu^{3+} with Thenoyltrifluoroacetonate, Sulfoxides and Macrocyclics. *J. Alloys Compd.* **1998**, *275*−*277*, 254−257.
(33) Campos, F. X.; Nascimento, A. L. C. S.; Colman, T. A. D.; Gálico, D. A.; Carvalho, A. C. S.; Caires, F. J.; Siqueira, A. B.; Ionashiro, M. Thermal Behavior, Spectroscopic Studies and Free Radical Scavenging Potential of Some Mefenamate Trivalent Lanthanides (Sm, Eu, Gd, Tb and Dy). *Thermochim. Acta* **2017**, *651*, 73−82.
(34) Deacon, G. B.; Phillips, R. J. Relationships between the Carbon-Oxygen Stretching Frequencies of Carboxylato Complexes and the Type of Carboxylate Coordination. *Coord. Chem. Rev.* **1980**, *33* (3), 227−250.
(35) Kaup, G.; Lezhnina, M. M.; Meiners, D.; Junk, P. C.; Kynast, U. H. Photophysical Properties of Rare Earth Diclofenac Complexes in the Solid State. *Aust. J. Chem.* **2015**, *68* (11), 1735−1740.
(36) Souza, A. P.; Rodrigues, L. C. V; Brito, H. F.; Alves, S.; Malta, O. L. Novel Europium and Gadolinium Complexes with Methaneseleninate as Ligand: Synthesis, Characterization and Spectroscopic Study. *Inorg. Chem. Commun.* **2012**, *15*, 97−101.
(37) Brito, H.F; Malta, O.L; Felinto, M.C.F.C; Teotonio, E.E.S; Menezes, J.F.S; Silva, C.F.B; Tomiyama, C.S; Carvalho, C.A.A Luminescence Investigation of the Sm(III)-β-Diketonates with Sulfoxides, Phosphine Oxides and Amides Ligands. *J. Alloys Cmpds.* **2002**, *344*, 293−297.
(38) Niyama, E.; Brito, H. F.; Cremona, M.; Teotonio, E. E. S.; Reyes, R.; Brito, G. E. S.; Felinto, M. C. F. C. Synthesis and Spectroscopic Behavior of Highly Luminescent Eu^{3+}-Dibenzoylmethanate (DBM) Complexes with Sulfoxide Ligands. *Spectrochim. Acta - Part A Mol. Biomol. Spectrosc.* **2005**, *61* (11−12), 2643−2649.
(39) Shannon, R. D.; Prewitt, C. T. Effective Ionic Radii in Oxides and Fluorides. *Acta Crystallogr. Sect. B Struct. Crystallogr. Cryst. Chem.* **1969**, *25* (5), 925−946.
(40) Shannon, R. D. Revised Effective Ionic Radii and Systematic Studies of Interatomic Distances in Halides and Chalcogenides. *Acta Crystallogr., Sect. A* **1976**, *32* (5), 751−767.
(41) Binnemans, K. Interpretation of Europium(III) Spectra. *Coord. Chem. Rev.* **2015**, *295*, 1−45.
(42) Zhuravlev, K. P.; Michnik, Ł.; Gawryszewska, P.; Tsaryuk, V. I.; Kudryashova, V. A. Europium and Terbium Pyrrole-2-Carboxylates: Structures, Luminescence, and Energy Transfer. *Inorg. Chim. Acta* **2019**, *492*, 1−7.
(43) Zhuravlev, K. P.; Tsaryuk, V. I.; Kudryashova, V. A. Photoluminescence of Europium and Terbium Trifluoroacetylacetonates. Participation of LMCT State in Processes of the Energy Transfer to Eu3+ Ion. *J. Fluor. Chem.* **2018**, *212*, 137−143.
(44) Lahoud, M. G.; Frem, R. C. G.; Gálico, D. A.; Bannach, G.; Nolasco, M. M.; Ferreira, R. A. S.; Carlos, L. D. Intriguing Light-Emission Features of Ketoprofen-Based Eu(III) Adduct Due to a Strong Electron-Phonon Coupling. *J. Lumin.* **2016**, *170*, 357−363.
(45) Faustino, W. M.; Malta, O. L.; de Sá, G. F. Theoretical Modeling of Thermally Activated Luminescence Quenching through Charge Transfer States in Lanthanide Complexes. *Chem. Phys. Lett.* **2006**, *429* (4−6), 595−599.
(46) Bünzli, J. C. G.; Comby, S.; Chauvin, A. S.; Vandevyver, C. D. B. New Opportunities for Lanthanide Luminescence. *J. Rare Earths* **2007**, *25* (3), 257−274.
(47) Carnall, W. T.; Crosswhite, H.; Crosswhite, H. M.*Energy Level Structure and Transition Probabilities in the Spectra of the Trivalent Lanthanides in LaF_3*; Argonne National Lab: Argonne, IL, 1978.
(48) Lima, G. B. V.; Bueno, J. C.; da Silva, A. F.; Carneiro Neto, A. N.; Moura, R. T.; Teotonio, E. E. S.; Malta, O. L.; Faustino, W. M. Novel Trivalent Europium β-Diketonate Complexes with N-(Pyridine-2-yl)Amides and N-(Pyrimidine-2-yl)amides as Ancillary Ligands: Photophysical Properties and Theoretical Structural Modeling. *J. Lumin.* **2020**, *219*, 116884.
(49) Moura, R. T.; Carneiro Neto, A. N.; Longo, R. L.; Malta, O. L. On the Calculation and Interpretation of Covalency in the Intensity Parameters of 4f−4f Transitions in Eu^{3+} Complexes Based on the Chemical Bond Overlap Polarizability. *J. Lumin.* **2016**, *170*, 420−430.
(50) Shyichuk, A.; Moura, R. T.; Neto, A. N. C.; Runowski, M.; Zarad, M. S.; Szczeszak, A.; Lis, S.; Malta, O. L. Effects of Dopant Addition on Lattice and Luminescence Intensity Parameters of Eu(III)-Doped Lanthanum Orthovanadate. *J. Phys. Chem. C* **2016**, *120* (50), 28497−28508.
(51) Carneiro, A. N.; Teotonio, E. E. S.; Sa, G. F.; De; Brito, H. F.; Legendziewicz, J.; Claudia, M.; Felinto, F. C.; Gawryszewska, P.; Moura, R. T.Modeling Intramolecular Energy Transfer in Lanthanide Chelates : A Critical Review and Recent Advances; *Handbook on the Physics and Chemistry of Rare Earths*; Elsevier, 2019; Vol. *56*, pp 55−162.
(52) Barthelemy, P. P.; Choppin, G. R. Luminescence Study of Complexation of Europium and Dicarboxylic Acids. *Inorg. Chem.* **1989**, *28* (17), 3354−3357.
(53) Rezende Souza, E.; Silva, I. G. N.; Teotonio, E. E. S.; Felinto, M. C. F. C.; Brito, H. F. Optical Properties of Red, Green and Blue Emitting Rare Earth Benzenetricarboxylate Compounds. *J. Lumin.* **2010**, *130* (2), 283−291.
(54) Latva, M.; Takalo, H.; Mukkala, V.-M.; Matachescu, C.; Rodríguez-Ubis, J. C.; Kankare, J. Correlation between the Lowest Triplet State Energy Level of the Ligand and Lanthanide(III) Luminescence Quantum Yield. *J. Lumin.* **1997**, *75* (2), 149−169.
(55) Lozano, J. J.; Pouplana, R.; López, M.; Ruiz, J. Conformational Analysis of the Antiinflammatory Fenamates: A Molecular Mechanics

https://doi.org/10.1021/acsaom.2c00070
ACS Appl. Opt. Mater. 2023, 1, 354−366

and Semiempirical Molecular Orbital Study. *J. Mol. Struct. THEOCHEM* **1995**, *335* (1−3), 215−227.
(56) Wittering, K. E.; Agnew, L. R.; Klapwijk, A. R.; Robertson, K.; Cousen, A. J. P.; Cruickshank, D. L.; Wilson, C. C. Crystallisation and Physicochemical Property Characterisation of Conformationally-Locked Co-Crystals of Fenamic Acid Derivatives. *CrystEngComm* **2015**, *17* (19), 3610−3618.
(57) Kovala-Demertzi, D.; Staninska, M.; Garcia-Santos, I.; Castineiras, A.; Demertzis, M. A. Synthesis, Crystal Structures and Spectroscopy of Meclofenamic Acid and Its Metal Complexes with Manganese(II), Copper(II), Zinc(II) and Cadmium(II). Antiproliferative and Superoxide Dismutase Activity. *J. Inorg. Biochem.* **2011**, *105* (9), 1187−1195.
(58) Jabeen, S.; Dines, T. J.; Leharne, S. A.; Chowdhry, B. Z. Spectrochimica Acta Part A : Molecular and Biomolecular Spectroscopy Raman and IR Spectroscopic Studies of Fenamates − Conformational Differences in Polymorphs of Flufenamic Acid, Mefenamic Acid and Tolfenamic Acid. *Spectrochim. Acta Part A Mol. Biomol. Spectrosc.* **2012**, *96*, 972−985.
(59) López-Mejías, V.; Kampf, J. W.; Matzger, A. *Nonamorphism in Flufenamic Acid and a New Record for a Polymorphic Compound with Solved Structures* **2012**, *134* (24), 9872−9875.
(60) Fonseca Guerra, C.; Sanz Miguel, P. J.; Cebollada, A.; Bickelhaupt, F. M.; Lippert, B. Rationalizing the Structural Variability of the Exocyclic Amino Groups in Nucleobases and Their Metal Complexes: Cytosine and Adenine. *Chem. - A Eur. J.* **2014**, *20* (31), 9494−9499.

NOTE ADDED AFTER ASAP PUBLICATION

This paper was published ASAP on November 16, 2022, with errors in Figure 9b. The corrected version was reposted on November 18, 2022.

https://doi.org/10.1021/acsaom.2c00070
ACS Appl. Opt. Mater. 2023, 1, 354−366